Charge storage mechanism of α-MnO$_2$ in protic and aprotic ionic liquid electrolytes

S. Lindberg [a], S. Jeschke [a], P. Jankowski [e,f], M. Abdelhamid [c], T. Brousse [b,d], J. Le Bideau [b,d], P. Johansson [a], A. Matic [a,*]

[a] Department of Physics, Chalmers University of Technology, S41296, Göteborg, Sweden
[b] Institut des Matériaux Jean Rouxel, Université de Nantes, CNRS UMR 650244322, Nantes Cedex 3, France
[c] Department of Chemistry - Ångström Laboratory, Uppsala University, Box 538, 751 21, Uppsala, Sweden
[d] Réseau sur le Stockage Electrochimique de l'Energie, CNRS FR 3459, 80039, Amiens Cedex, France
[e] Technical University of Denmark, Department of Energy Conversion and Storage, 2800, Kgs Lyngby, Denmark
[f] Warsaw University of Technology, Faculty of Chemistry, 00-664, Warsaw, Poland

HIGHLIGHTS

- Hydrogen bonding between MnO$_2$ and an IL cation important for charge storage.
- A faradaic contribution from MnO$_2$ is observed with a protic IL, due to a redox reaction.
- Capacity explained by a densely packed layer of standing cations on the surface.
- For aprotic ILs only double layer charge storage is observed.

ARTICLE INFO

ABSTRACT

In this work we have investigated the charge storage mechanism of MnO$_2$ electrodes in ionic liquid electrolytes. We show that by using an ionic liquid with a cation that has the ability to form hydrogen bonds with the active material (MnO$_2$) on the surface of the electrode, a clear faradaic contribution is obtained. This situation is found for ionic liquids with cations that have a low pKa, i.e. protic ionic liquids. For a protic ionic liquid, the specific capacity at low scan rate rates can be explained by a densely packed layer of cations that are in a standing geometry, with a proton directly interacting through a hydrogen bond with the surface of the active material in the electrode. In contrast, for aprotic ionic liquids there is no interaction and only a double layer contribution to the charge storage is observed. However, by adding an alkali salt to the aprotic ionic liquid, a faradaic contribution is obtained from the insertion of Li$^+$ into the surface of the MnO$_2$ electrode. No effect can be observed when Li$^+$ is added to the protic IL, suggesting that a densely packed cation layer in this case prevent Li-ions from reaching the active material surface.

1. Introduction

There is a growing interest in the application of supercapacitors (SCs) spurred by their power and cycle performance. However, to meet the specifications of many emerging applications, an increase in the energy content is required [1]. To increase the energy density, the addition of redox active materials to the electrodes has been explored in hybrid supercapacitor devices [2]. The redox active material adds a faradaic contribution to the charge storage in the electrode that is in addition to the double layer capacitance of a traditional SC. A commonly explored route is the addition of transition metal oxides to the electrode [3–5], and among these MnO$_2$ is considered one of the most promising redox materials due to a high theoretical capacitance and high natural abundance [5].

In MnO$_2$ based electrodes, for hybrid SCs, the mechanisms involved in charge storage are a redox reaction (Mn(III) to Mn(IV)), and electrical double-layers at the surface of the electrode [6–8]. Most commonly, MnO$_2$ type electrodes are used in combination with aqueous

---

* Corresponding author.
  E-mail address: matic@chalmers.se (A. Matic).

electrolytes, where the faradaic process originates from the electrochemical reaction between protons in the electrolyte and the transition metal oxide [9]. However, MnO_2 is not stable in acidic electrolytes as it forms soluble MnOOH species [10]. To improve the stability, neutral electrolytes containing alkali metal cations, e.g. Li^+, are used, with a faradaic charge storage mechanism based on electrochemical reactions that utilize both protons and the alkali metal cation [7,11]. Even though the use of aqueous based electrolytes can provide good cyclability, dissolution of MnO_2 complexes can still occur at neutral conditions. In addition, the voltage window of the device is limited to around 1–1.3 V by the water splitting at 1.23 V vs SHE [9].

To address both the dissolution of active material and the limited potential window, ionic liquids (ILs) are considered as promising alternatives. ILs are salts with a melting point below 100 °C, often considerably below room temperature [12,13]. By the proper selection of the anion and cation several families of ionic liquids with high electrochemical stability (up to 5 V), non-flammability, and low vapor pressure have been developed. The wider potential window results in an increased energy density and with respect to faradaic electrode materials the solubility of metal oxides is usually lower in ionic liquids [14], which could improve cyclability.

In the case of protic ionic liquids (PILs), protons on the cation can be available for electrochemical interactions with a faradaic material [15], which could enable a similar mechanism as present with aqueous electrolytes. There has been only a few studies using PILs in combination with e.g. RuO_2 or MnO_2 electrodes [16,17], showing that redox-transitions took place with protons transferred from the electrolyte to the electrode. However, in these studies the electrolyte contained an excess amount of acid, thus it was not a true ionic liquid, and the proton activity could also be related to the acid. There is still an interest to understand potential mechanisms of proton interaction with a faradaic material using true ionic liquid electrolytes. In addition, the role of alkali metal cations in the electrochemical processes when using an ionic liquid has not been investigated in hybrid SCs. Ionic liquids can readily dissolve typical Li-metal salts and Li-ion containing ionic liquid electrolytes have been explored for Li-battery applications [12,13].

In this work we target the mechanism of interaction between ionic liquids and the faradaic material MnO_2. Specifically, we target how the proton availability influences the electrochemical response. To address this issue, we use ionic liquid electrolytes with the same anion, but with cations varying only in slight modifications of the side chain of the cation, see Fig. 1, resulting in different proton donor ability. In addition, we investigate the influence of the presence of alkali metal cations by adding LiTFSI to the ionic liquids. The electrochemical response of MnO_2 electrodes previously studied in aqueous electrolytes [11], is here investigated with these ionic liquid electrolytes and the mechanism discussed in relation to the proton availability, interaction energies, and geometry. We show that in the case where there is the possibility to form a hydrogen bond, the proton on the cation can interact electrochemically with MnO_2. At the same time this interaction efficiently blocks interaction between Li^+ and the MnO_2.

2. Experimental

2.1. Electrolytes

1-ethyl-3-methylimidazolium bis(trifluoromethane)sulfonamide (EMIM TFSI, 99.5%), 1-ethanol-3-methylimidazolium bis(trifluoromethane)sulfonamide (EtOHIM TFSI, 99%) and lithium bis(trifluoromethane)sulfonamide (LiTFSI, 99.9%) were purchased from Solvionic, and 1-ethylimidazolium bis(trifluoromethane)sulfonamide (EIM TFSI, 98%) from Iolitec. All chemicals were used as received.

2.2. MnO₂ electrode preparation

α-MnO_2 (cryptomelane phase) was obtained from ERACHEM (MnO_2 HSSA). The structure and morphology of this material has been reported previously from XRD [18] and SEM characterization [19]. The MnO_2 electrodes were prepared following a previously reported procedure [20], in brief, MnO_2 (75 wt%), PTFE (5 wt%), and carbon black (20 wt %) were mixed in ethanol. The slurry was pressed slightly and left to dry to form a film. The film was pressed between two stainless steel meshes at 9000 MPa for 60 min. The geometrical electrode area was about 0.25 cm^2 and the mass loading was 7 mg/cm^2.

2.3. Electrochemical measurements

The electrochemical measurements were performed in 3-electrode T-shaped polystyrene Swagelok cells with stainless steel rods as current collectors and using a PalmSense3 potentiostat. Activated carbon was used as counter electrode and glass fiber paper (Whatman, 0.26 mm) was used as separator. Silver foil (Alfa Aesar, 99.9%) was used as quasi-reference electrode (QRE). The silver foil was polished with an alumina slurry (30 μm particles), ultrasonicated in MilliQ water, acetone and finally ethanol for 10 min each, respectively. The potential of the Ag/Ag^+- QRE was determined by adding 0.02 M of ferrocene (FCE) to the different electrolytes and cycling the cells at 20 mV s^{-1}. The reduction and oxidation potentials established for FCE in the different ILs can be found in the supporting information, Table S1.

2.4. Electrolyte characterization

Ionic conductivities were determined with a Novocontrol dielectric spectrometer using a coin cell with stainless steel electrodes and glass fiber separator (0.26 mm). The viscosities were measured at 20 °C with an Anton Paar LOVIS 2000 M micro-viscometer with the falling ball method, using a stainless-steel ball with a density of 7.7 g cm^{-3} and a capillary with an inner diameter of 1.6 mm for low viscosity samples and 2.8 mm for high viscosity samples. The water content in the ionic liquids and LiTFSI salt was determined by Karl-Fischer titration and is presented in Table S3.

2.5. Calculations

Theoretical pKa-values of the different cations were calculated as if they were alone in water. The protons used in the calculations are indicated in Fig. 2. The calculations were performed using the Conductor-like Screening Model for Real Solvents (COSMO-RS), a computational method that integrates concepts of quantum chemistry, dielectric continuum models, electrostatic surface interactions, and statistical thermodynamics to predict thermodynamic quantities and equilibria of fluids and liquid mixtures [21,22]. The molecular structures of the imidazolium compounds and their corresponding deprotonated zwitter-ion for the initial quantum chemical step were built in the graphical user interface TmolX 4.2, and the calculations were performed with the TURBOMOLE V7.1 [23,24] program package. Geometries were optimized using the BP86-functional [25,26] and TZVP basis set [27] in the gaseous phase and for the perfect conductor (COSMO: ε = ∞).
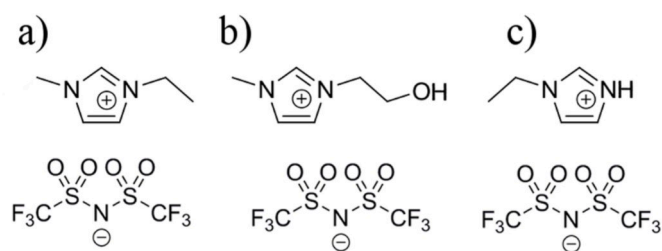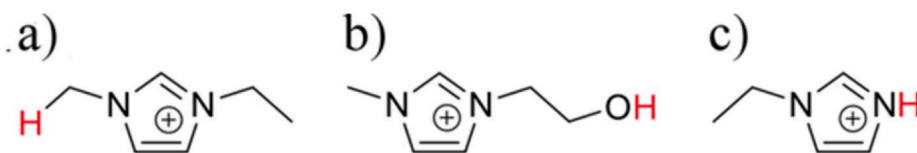

Fig. 1. Structures of ions of the investigated ionic liquids a) 1-ethyl-3-methylimidazolium TFSI, b) 1-ethanol-3-methylimidazolium TFSI, c) 1-ethylimidazolium TFSI.

Fig. 2. The protons on the cations used in the COSMO-RS calculations (red) for a) EMIM, b) EtOHIM, and c) EIM. (For interpretation of the references to colour in this figure legend, the reader is referred to the Web version of this article.)

Additionally, a single point calculation at BP86/TZVPD//BP86/TZVP level of theory was performed for the gaseous and the COSMO phase in order to generate a fine grid cavity (FINE) for the molecules. The COSMO-RS calculations were performed with the COSMOthermX program [28], using the BP_TZVPD_FINE_C30_1701 parameterization at 298.15 K. The pKa module was used to compute the pKa values with the "parameters for -acid- in solvent" settings for water and acetonitrile (ACN), and "parameters for -base- in solvent" settings for water and ACN.

The interaction energy between a 110 MnO_2 surface and the cations of the ionic liquids were calculated using Density Functional Theory (DFT). All DFT electronic structure calculations were performed using Vienna ab-initio Simulation Package (VASP) [29], employing the PBE exchange-correlation functional with Hubbard U corrections (U_{Eff} = 3.90 eV) and projector augmented wave (PAW) potentials for all elements. An energy cut-off of 520 eV was imposed for the plane wave basis set. The 110-surface of MnO_2 was constructed from the primitive cell using double layers containing 6 × 4 manganese atoms, a Gamma-centered 2 × 3 × 2 k-mesh was used as grid. Geometry and cell parameter optimization were performed using a convergence criterion set to 0.01 eV Å^{-1}. The cations (EIM, EtOHIM and EMIM) were added in close proximity to the optimized surfaces in two different positions in order to investigate geometries where the imidazole ring on the cations is oriented parallel or perpendicular to the surface. Geometries were reoptimized and the ones with the lowest energy are considered in this study.

3. Results and discussion

To investigate the electrochemical response of MnO_2 in neat ionic liquid electrolytes, cyclic voltammetry (CV) experiments were performed in the potential window 0–1.1 V at increasing scan rates (1–20 mV s^{-1}). Fig. 3 shows the results at the lowest and the highest scan rates. For EMIM TFSI, the typical rectangular profiles and low specific currents indicate a double layer capacitance type of charge storage [30], without any faradaic contribution from the MnO_2 in the electrode. A similar response is observed for EtOHIM, however with a slight tilt of the CV curve reflecting an increased resistance in the electrolyte, related to the higher viscosity and lower conductivity compared to EMIM TFSI, see Table S2 in supplementary information. In contrast, for the protic ionic liquid EIM TFSI, a clear faradaic peak centered at 0.6 V vs Ag/Ag$^+$ is observed in the CV during oxidation at a low scan rate (1 mV s^{-1}). This peak's counterpart during reduction has an onset around 0.6 V and extends down to 0 V vs Ag/Ag$^+$. At 20 mV s^{-1} there is still an indication of a peak around 0.8 V in the oxidation scan. The less pronounced peak and the shift in position indicates that the kinetics are rather slow and that the relative contribution from capacitive charge storage has increased [31]. The pronounced tilt of the CV curve at 20 mV s^{-1} can also here be ascribed to a low conductivity.

To explain the differences in the CVs for the three ionic liquids we can consider both their physical properties and their possibilities to interact with the active material, MnO_2, in the electrode. In the absence of any other cation the possibility of an available proton on the cation could induce a redox reaction similar to [9]:

$$Mn(IV)O_2 + H^+ + e^- \Rightarrow Mn(III)OOH \qquad (1)$$
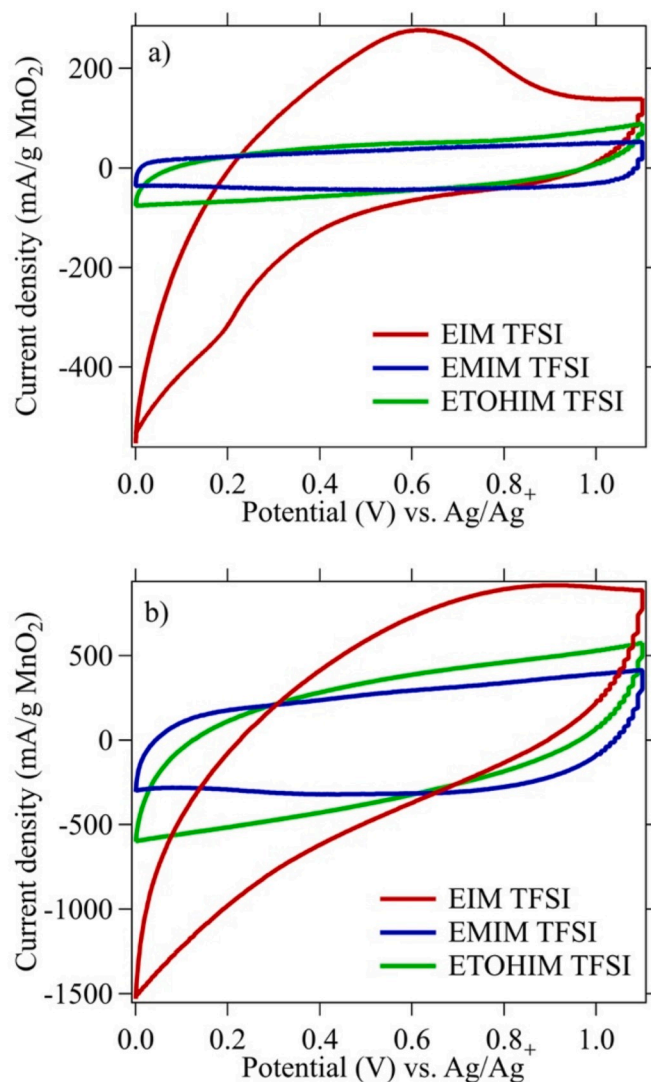
Fig. 3. Cyclic voltammograms of MnO_2 electrodes in neat EIM TFSI, EMIM TFSI, and EtOHIM TFSI at a) 1 mV s^{-1}, and b) 20 mV s^{-1}.

$$Mn(III)OOH \Rightarrow Mn(IV)O_2 + H^+ + e^- \qquad (2)$$
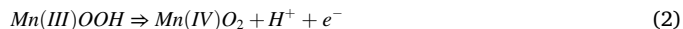
Here the ability to donate protons would allow reduction/oxidation of the Mn-ion. EIM TFSI is a protic IL, according to the definition that it is formed through the reaction and proton transfer between a Brønsted acid and Brønsted base [32]. The transferred proton can potentially be donated or form a hydrogen bond [33]. EtOHIM TFSI is not a protic IL but rather a Brønsted acidic IL with an OH-group on the cation, which could potentially interact with the surface. EMIM TFSI is considered as an aprotic IL, with no ability to donate protons. Table 1 shows pKa-values from COMSO-RS calculations for the three cations. A small pKa-value indicates that a cation is more prone to create hydrogen bonds and donate protons, even though some proton interaction still can occur

Table 1
PKa-values from COSMO-RS calculations for the different cations in water.

	EIM	EtOHIM	EMIM
Water	8.1	13.7	28.2

at higher pKa-values [34]. These results show that the EMIM and EtO-HIM cations are much weaker proton donors, compared to EIM, and are thus not prone to interact with MnO$_2$. Thus, the faradaic contribution to the CV when using EIM TFSI as the electrolyte can be assigned to an interaction between the proton on the cation and MnO$_2$. Potentially, there is the formation of MnOOH-type species, according to the reactions in (1) and (2), without the proton actually detaching from the cation. Support for this scenario is provided by the small kink in the CV at 0.2 V during reduction which as previously been assigned to the dissolution of MnOOH complexes [10].

To further understand the interaction of the cations with the MnO$_2$ material and the CV response, Fig. 3, adsorption energies for the cations on a MnO$_2$-110 surface were calculated by DFT. Two different geometries, flat and standing with respect to the plane of the imidazole ring, were investigated, as shown in Fig. 4. For each cation the flat configuration provides the strongest interaction, a result which is in line with previous theoretical work for other surfaces and the EMIM cation [35, 36]. For the flat geometry EIM shows the highest interaction energy, as expected from the pKa values, as a result of the interaction between the -NH group and oxygens on the MnO$_2$ surface. This interaction induces in a tilt of the ion with respect to the surface, indicating the formation of a hydrogen bond which increases the adsorption energy. For the other two ions this effect is not observed. EtOHIM shows the lowest adsorption energy, which can be explained by the lower charge of the aromatic ring. The -OH group is not able to form a hydrogen bond in this configuration, and in that way increase the interaction energy.

The flat geometry is quite a dilute configuration and in an ionic liquid electrolyte the ion-ion interaction might favor other geometries. A standing geometry would allow a more efficient packing of the ions on the surface and could thus be favored. The results from the DFT calculations show that also in this geometry the EIM ion has the highest adsorption energy, and that there is a direct interaction between the

proton on the -NH group and the oxygen on the surface. This configuration allows hydrogen bonding and, in this way, a path for electron transfer when lowering the potential. EtOHIM has the second highest interaction energy in the standing geometry, but there is still no direct hydrogen bonding interaction between the -OH group and the surface, since the OH-group is not pointing towards the surface for the optimized geometry. These results show that the interaction energy depends on the geometry and that the pKa-values from the COSMO RS calculations cannot be directly translated to an interaction with the surface if the hydrogen-bonding is too weak.

With the addition of Li$^+$ to the electrolyte a second mechanism for a faradaic contribution is possible according to:

$$Mn(III)OOLi \Rightarrow Mn(IV)O_2 + Li^+ + e^- \tag{3a}$$

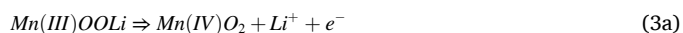$$Mn(IV)O_2 + Li^+ + e^- \Rightarrow Mn(III)OOLi \tag{3b}$$

Fig. 5 shows the effect on the CVs when adding LiTFSI to the ionic liquid electrolytes. In the case of EMIM TFSI the non-faradaic response in the neat IL turns into a faradaic response with a broad oxidation peak, from 0.1 to 0.9 V, and an increased current during reduction at a low scan rate. Similarly, the addition of LiTFSI to EtOHIM TFSI also leads to a faradaic contribution, with an oxidation peak centered around 0.5 V, and the onset of a faradaic current around 0.5 V at reduction. The increase in the peak current caused by the addition of LiTFSI is much smaller in the case of EtOHIM compared to EMIM TFSI, and is probably a result of the much higher viscosity (lower conductivity) of EtOHIM, see Table S2. Thus, for these two electrolytes there is clearly a contribution from an interaction between Li$^+$ and MnO$_2$, as proposed by the reaction schemes 3a-b.

In the case of the protic ionic liquid EIM TFSI the faradaic contribution observed in the CV of the neat IL electrolytes is in fact reduced by the addition of LiTFSI. One could envisage having both Li$^+$ and the EIM cation interacting with MnO$_2$ in the electrode according to [7].

$$Mn(IV)O_2 + xLi^+ + yH^+ + (x+y)e^- \Rightarrow xMn(III)OOLi + yMn(III)OOH$$
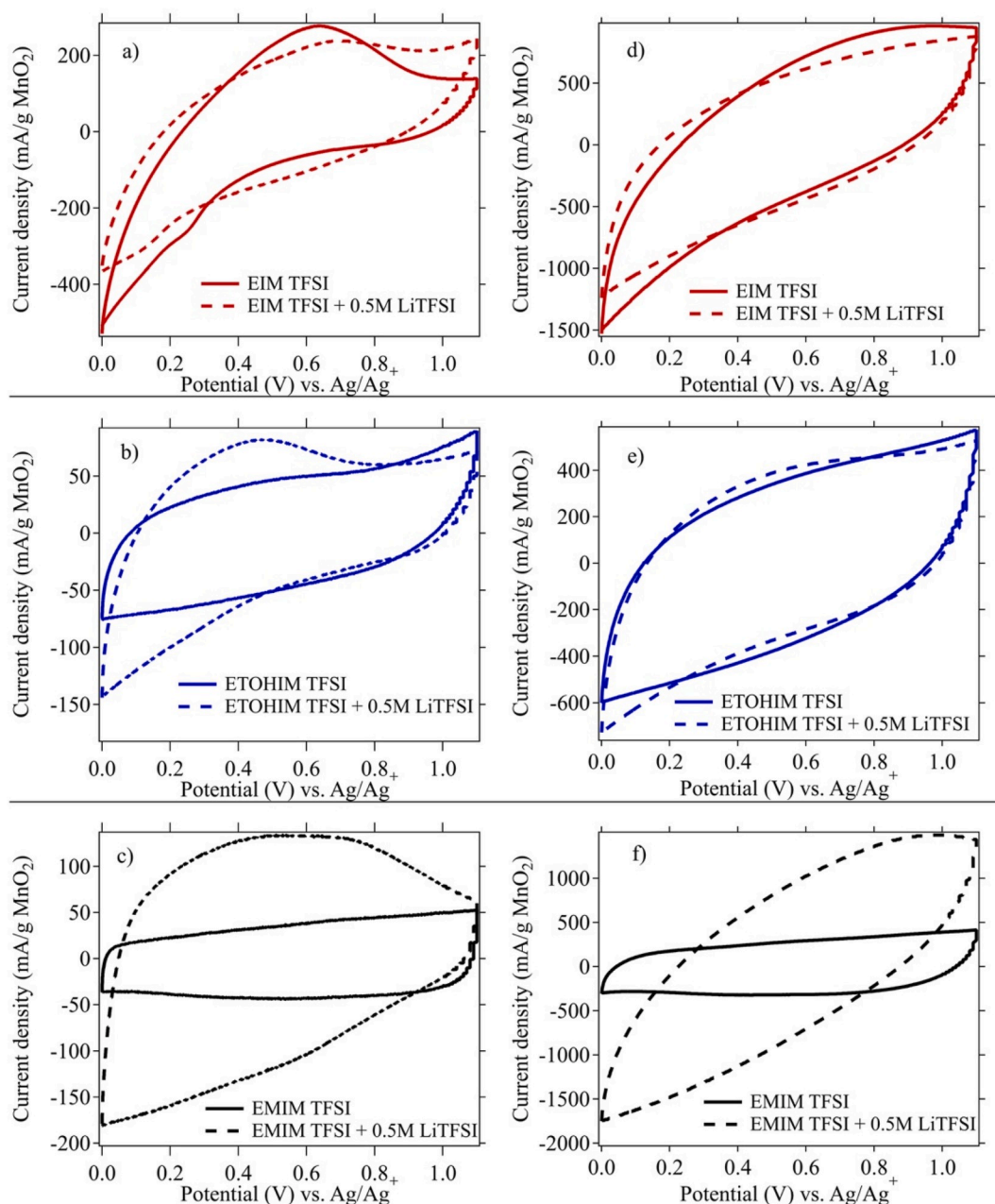$$\tag{4}$$
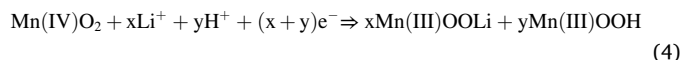
However, the shape of the CV curve, with a slight decrease in the oxidation peak at 0.6 V and the absence of the peak around 0.5 V,
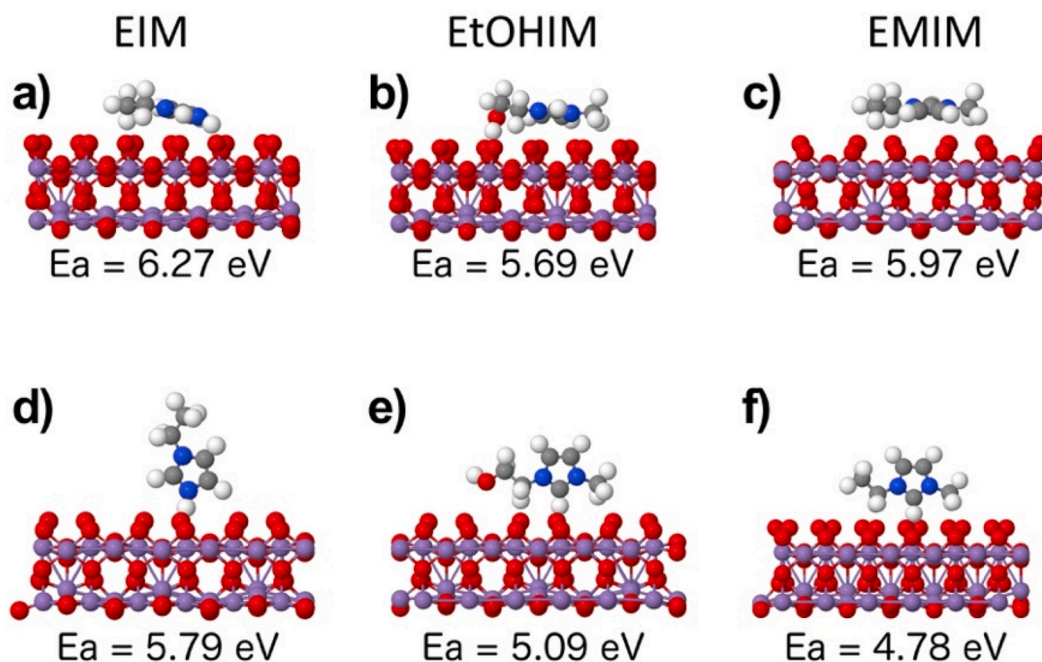
Fig. 4. Optimized geometries from DFT calculations for flat (a-c) and standing (d-f) configurations, respectively. Calculated adsorption energy (eV) for each configuration is shown in the figure.

Fig. 5. Cyclic voltammograms of MnO$_2$ electrodes with a) EIM TFSI b) EtOHIM TFSI c) EMIM TFSI at 1 mV s^{-1}(left) and 20 mV s^{-1} (right) with and without the addition of 0.5 M LiTFSI.

corresponding to Li$^+$ insertion, suggests that it is still mainly protons that provide the faradaic contribution in the case of the EIM TFSI/LiTFSI electrolyte. The overall lower current response can be explained by a lower conductivity with the addition of LiTFSI, see Table S2.

At a high scan rate, 20 mV s^{-1}, the CVs for the EIM TFSI/LiTFSI and EtOHIM TFSI/LiTFSI electrolytes are very similar to what is found for the neat ionic liquid electrolytes. In contrast, a very large increase in the current response, as well as tilt of the CV curve, is found for EMIM TFSI/LiTFSI. This change can be ascribed to the fact that the faradaic contribution is still dominating, but that there is an increased resistance. This increased resistance can be ascribed to a change in the charge storage mechanism, as it changes from double layer capacitance to a slower faradaic contribution as well as a decrease in the conductivity of the electrolyte with the addition of LiTFSI.

In order to compare the contribution of MnO$_2$ to the capacity for the different electrolytes at different scan speeds, the specific capacity (mAh

g^{-1}) was calculated by integrating the reduction current of the cyclic voltammograms according to:

$$Specific\ capacity\ \left(mAh\ g^{-1}\right) = 1 \left/ vW \int_{V_1}^{V_2} iVdV \right. \tag{5}$$

Here v is the scan speed (V s^{-1}), W mass of active material (g) and V$_1$ and V$_2$ define the potential region of the reduction current [11]. Fig. 6a shows the calculated specific capacities for the MnO$_2$ electrodes when used together with the three different ionic liquids, without and with the addition of LiTFSI. The theoretical capacity for a single electron process in MnO$_2$ is 308 mA h g^{-1}. However, due to the low electronic conductivity of MnO$_2$ only a fraction of the theoretical capacity is achieved in practice. For EIM TFSI the calculated capacity is about 12% of the theoretical value, suggesting that only a thin surface layer on the MnO$_2$ particles in the electrode is involved in the charge storage process. For
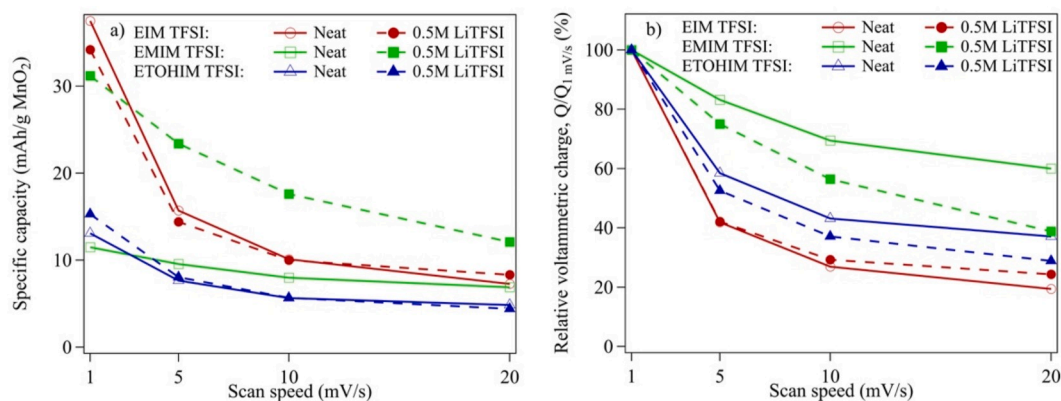
Fig. 6. a) Specific capacity and b) relative voltammetric charge of MnO_2 electrodes with the different ionic liquids, with and without LiTFSI. Lines are guides to the eye.

neat EMIM TFSI and EtOHIM TFSI the capacity is only 3–4% of the theoretical capacity of MnO_2. This capacity translates into an average capacitance of 43 F g^{-1} or 36 μF cm^{-2}, according to the specific surface area of the MnO_2 material (130 m^2 g^{-1}) [37]. Although it is not strictly correct to calculate a capacitance which is not quite constant over the whole potential window, it still provides an estimate [38], and the obtained result is in good agreement with a double layer capacitance for oxide or metal electrodes [3,39], and is also consistent with the absence of faradaic signatures in the CV. It can be noted that when LiTFSI is added to EMIM TFSI the capacity is again found to be around 12% of the theoretical one and we can envisage insertion of Li^+ in a thin surface layer on MnO_2 particles, as in the case of proton interaction with the protic IL.

To link the calculated capacity to possible geometries of the ions on the MnO_2 surface, we can evaluate how densely the EIM cations need to be packed to deliver the stored charge as a result of a faradaic surface process. We can here consider the flat and standing geometries investigated in the DFT calculations. From the projected areas of the EIM ion on the surface in the optimized configurations from DFT calculations (0.18 nm^2 and 0.32 nm^2 for the standing and flat configurations respectively), and by the specific surface area of the MnO_2 material (130 m^2/g) a specific capacity of 18 mA h/g (with respect to the weight of MnO_2) is obtained for the flat geometry, and 31 mA h/g (10% of the theoretical capacity) for the standing geometry, assuming 1 e^-/cation. Thus, a faradaic contribution from a reaction between protons and MnO_2 with cations in the standing geometry together with a double layer contribution accounts well for the experimentally observed total capacity, 37 mA h/g at low scan rate.

In Fig. 6b the relative voltammetric charge is shown as a function of scan speed [20]. For all ionic liquid electrolytes there is capacity fade with increased scan speed, as can be expected from their relatively high viscosities (low conductivities). However, the capacity retention for EMIM TFSI is significantly better and the capacity increases considerably when LiTFSI is added. At high scan speeds it shows the highest capacity among all the tested electrolytes. The difference in capacity and capacity retention can be sought in the interaction of the ions with the MnO_2, and the physical properties of the ILs. For neat EMIM TFSI the totally dominant contribution to the capacity comes from the formation of a double layer capacitance, which can be seen from the rectangular CV profiles, Fig. 4c,f. This is also underlined by the good capacity retention, which is often the case for double layer capacitance. Adding Li^+ to EMIM TFSI enables a faradaic contribution to the capacity from the MnO_2 at slower scan speeds. Consequently, the capacity retention is reduced as a result of the faradaic contribution being dominant. In the case of EIM TFSI the availability of protons leads to a preferential interaction of the cation with the MnO_2 surface. This interaction blocks a potential interaction of Li^+ with MnO_2 that could increase the capacity

as well as to the formation a dense double layer that would contribute to the capacity at high scan rates.

4. Conclusions

We have investigated the interaction between ionic liquid cations and the faradaic material MnO_2 to understand the possibility to exploit redox contributions to the total capacity in hybrid supercapacitors with ionic liquid electrolytes. We show that a faradaic contribution when using neat ionic liquid electrolytes and MnO_2 electrodes is determined by the chemical groups that are attached to the cations. When the cation has the possibility to form a hydrogen bond with the active material on the surface of the electrode there can be a direct interaction. This is evident when comparing the electrochemical response in cyclic voltammetry for protic and aprotic ionic liquids. The cation in the protic ionic liquid EIM TFSI has a lower pKa-value and a stronger adsorption energy at the MnO_2 surface, compared to the aprotic ionic liquid, which enables it to be electrochemically active. There is a direct interaction with the MnO_2 surface through the formation of a hydrogen bond.

The specific capacity at low scan rates is well explained by a configuration where cations adsorb to the MnO_2 surface in a standing geometry, with the -NH group on the cation participating in the redox process. For a neat aprotic ionic liquid there is no faradaic contribution, and only an electrical double layer mechanism for charge storage is observed. However, by the addition of Li^+ to the aprotic ionic liquid a faradaic contribution is triggered and can be explained by the insertion of Li^+ in MnO_2. No synergistic effect of protons and Li^+ can be found for the protic ionic liquid, suggesting that the cations efficiently block the access to the surface for the alkali ions. Overall our results show that a faradaic contribution can be exploited also at high scan rates when using ionic liquids, but that the relatively low conductivity of the electrolyte limits the high-power performance. Thus, to take ionic liquid-based electrolytes towards application, new systems with high conductivity (low viscosity) need to be developed. Alternatively, one can consider the addition of a small fraction of organic solvents in order to improve the conductivity. It has previously been shown for Li-batteries that the addition of a small amount of organic solvent improves the performance without sacrificing the unique properties of ionic liquids in terms of electrochemical and thermal stability [40], and this might also be a viable way forward in hybrid supercapacitor applications.

Declaration of competing interest

The authors declare that they have no known competing financial interests or personal relationships that could have appeared to influence the work reported in this paper.

CRediT authorship contribution statement

S. Lindberg: Investigation, Formal analysis, Conceptualization, Writing - original draft. **S. Jeschke:** Investigation, Formal analysis, Writing - review & editing. **P. Jankowski:** Investigation, Formal analysis, Writing - review & editing. **M. Abdelhamid:** Writing - review & editing, Resources, Supervision. **T. Brousse:** Writing - review & editing, Resources. **J. Le Bideau:** Writing - review & editing, Resources. **P.**

Johansson: Writing - review & editing. **A. Matic:** Writing - review & editing, Supervision, Conceptualization, Project administration.

Appendix A. Supplementary data

Supplementary data to this article can be found online at https://doi.org/10.1016/j.jpowsour.2020.228111.

Supplementary information

Oxidation and reduction potentials of ferrocene (FCE) in the ILs.

Table S1
Oxidation and reduction potentials of ferrocene in the ionic liquid electrolytes.

	Oxidation and reduction potentials of FCE (mV)		
	EMIM TFSI	EIM TFSI	EtOHIM TFSI
Ox/Red	−429/+785	−258/+179	−334/+605

Viscosity and conductivity

The viscosities and conductivities of the neat ILs and with 0.5 M LiTFSI are reported in Table S2.

Table S2
Measured viscosities (mPa s) and conductivities (mS cm^{-1}) of the neat ILs and when adding 0.5 M LiTFSI, at R.T.

	Viscosity (mPa s)		
	EMIM TFSI	EIM TFSI	EtOHIM TFSI
Neat	24.1	42.1	82.9
+ 0.5M LiTFSI	39.8	75.0	207
Conductivity (mS cm^{-1})			
Neat	7.3	2.5	1.8
+ 0.5M LiTFSI	3.1	2.3	0.9

Water content.

Table S3
Water content (ppm) the ILs and LiTFSI.

	Water content (ppm)			
	EMIM TFSI	EIM TFSI	EtOHIM TFSI	LiTFSI
Water content	320	<20	538	6

References

[1] C. Schütter, S. Pohlmann, A. Balducci, Industrial requirements of materials for electrical double layer capacitors: impact on current and future applications, Adv. Energy Mater. 9 (2019) 1900334, https://doi.org/10.1002/aenm.201900334.

[2] A. González, E. Goikolea, J.A. Barrena, R. Mysyk, Review on supercapacitors: technologies and materials, Renew. Sustain. Energy Rev. 58 (2016) 1189–1206, https://doi.org/10.1016/J.RSER.2015.12.249.

[3] W. Sugimoto, T. Kizaki, K. Yokoshima, Y. Murakami, Y. Takasu, Evaluation of the pseudocapacitance in RuO$_2$ with a RuO$_2$/GC thin film electrode, Electrochim. Acta 49 (2004) 313–320, https://doi.org/10.1016/j.electacta.2003.08.013.

[4] N.M. Ndiaye, T.M. Masikhwa, B.D. Ngom, M.J. Madito, K.O. Oyedotun, J. K. Dangbegnon, N. Manyala, Effect of growth time on solvothermal synthesis of vanadium dioxide for electrochemical supercapacitor application, Mater. Chem. Phys. 214 (2018) 192–200, https://doi.org/10.1016/j.matchemphys.2018.04.087.

[5] Q.Z. Zhang, D. Zhang, Z.C. Miao, X.L. Zhang, S.L. Chou, Research progress in MnO$_2$–carbon based supercapacitor electrode materials, Small 14 (2018) 1–15, https://doi.org/10.1002/smll.201702883.

[6] D. Bélanger, T. Brousse, J.W. Long, Manganese oxides: battery materials make the leap to electrochemical capacitors, Electrochem. Soc. Interface. 17 (2008) 49–52.

[7] M. Toupin, T. Brousse, D. Bélanger, Charge storage mechanism of MnO$_2$ electrode used in aqueous electrochemical capacitor, Chem. Mater. 16 (2004) 3184–3190, https://doi.org/10.1021/cm049649j.

[8] D. Chen, D. Ding, X. Li, G.H. Waller, X. Xiong, M.A. El-Sayed, M. Liu, Probing the charge storage mechanism of a pseudocapacitive MnO$_2$ electrode using in operando Raman spectroscopy, Chem. Mater. 27 (2015) 6608–6619, https://doi.org/10.1021/acs.chemmater.5b03118.

[9] C. Zhong, Y. Deng, W. Hu, J. Qiao, L. Zhang, J. Zhang, A review of electrolyte materials and compositions for electrochemical supercapacitors, Chem. Soc. Rev. 44 (2015) 7484–7539, https://doi.org/10.1039/C5CS00303B.

[10] S. Bodoardo, J. Brenet, M. Maja, P. Spinelli, Electrochemical behaviour of MnO$_2$ electrodes in sulphuric acid solutions, Electrochim. Acta 39 (1994) 1999–2004, https://doi.org/10.1016/0013-4686(94)85080-1.

[11] N. Goubard-Bretesché, O. Crosnier, G. Buvat, F. Favier, T. Brousse, Electrochemical study of aqueous asymmetric FeWO$_4$/MnO$_2$ supercapacitor, J. Power Sources 326 (2016) 695–701, https://doi.org/10.1016/j.jpowsour.2016.04.075.

[12] M. Armand, F. Endres, D.R. MacFarlane, H. Ohno, B. Scrosati, Ionic-liquid materials for the electrochemical challenges of the future, Nat. Mater. 8 (2009) 621–629, https://doi.org/10.1038/nmat2448.

[13] A. Matic, B. Scrosati, Ionic liquids for energy applications, MRS Bull. 38 (2013) 533–537, https://doi.org/10.1557/mrs.2013.154.

[14] J.K. Kim, C.R. Shin, J.H. Ahn, A. Matic, P. Jacobsson, Highly porous $LiMnPO_4$ in combination with an ionic liquid-based polymer gel electrolyte for lithium batteries, Electrochem. Commun. 13 (2011) 1105–1108, https://doi.org/10.1016/j.elecom.2011.07.005.

[15] A.S. Amarasekara, Acidic ionic liquids, Chem. Rev. 116 (2016) 6133–6183, https://doi.org/10.1021/acs.chemrev.5b00763.

[16] L. Mayrand-Provencher, D. Rochefort, Influence of the conductivity and viscosity of protic ionic liquids electrolytes on the pseudocapacitance of RuO_2 electrodes, J. Phys. Chem. C 113 (2009) 1632–1639, https://doi.org/10.1021/jp8084149.

[17] C.A. Castro Ruiz, D. Bélanger, D. Rochefort, Electrochemical and spectroelectrochemical evidence of redox transitions involving protons in thin MnO_2 electrodes in protic ionic liquids, J. Phys. Chem. C 117 (2013) 20397–20405, https://doi.org/10.1021/jp405047g.

[18] R. Zhang, X. Yu, K.W. Nam, C. Ling, T.S. Arthur, W. Song, A.M. Knapp, S. N. Ehrlich, X.Q. Yang, M. Matsui, α-MnO_2 as a cathode material for rechargeable Mg batteries, Electrochem. Commun. 23 (2012) 110–113, https://doi.org/10.1016/j.elecom.2012.07.021.

[19] A. Boisset, L. Athouël, J. Jacquemin, P. Porion, T. Brousse, M. Anouti, Comparative performances of birnessite and cryptomelane MnO_2 as electrode material in neutral aqueous lithium salt for supercapacitor application, J. Phys. Chem. C 117 (2013) 7408–7422, https://doi.org/10.1021/jp3118488.

[20] T. Brousse, M. Toupin, R. Dugas, L. Athouël, O. Crosnier, D. Bélanger, Crystalline MnO_2 as possible alternatives to amorphous compounds in electrochemical supercapacitors, J. Electrochem. Soc. 153 (2006) A2171, https://doi.org/10.1149/1.2352197.

[21] A. Klamt, F. Eckert, COSMO-RS: a novel and efficient method for the a priori prediction of thermophysical data of liquids, Fluid Phase Equil. 172 (2000) 43–72, https://doi.org/10.1016/S0378-3812(00)00357-5.

[22] A. Klamt, F. Eckert, M. Diedenhofen, M.E. Beck, First principles calculations of aqueous pKa values for organic and inorganic acids using COSMO-RS reveal an inconsistency in the slope of the pKa scale, J. Phys. Chem. 107 (2003) 9380–9386, https://doi.org/10.1021/jp034688o.

[23] TURBOMOLE, (2015).

[24] R. Ahlrichs, M. Bär, M. Häser, H. Horn, C. Kölmel, Electronic structure calculations on workstation computers: the program system turbomole, Chem. Phys. Lett. 162 (1989) 165–169, https://doi.org/10.1016/0009-2614(89)85118-8.

[25] J.P. Perdew, Density-functional approximation for the correlation energy of the inhomogeneous electron gas John, Phys. Rev. B 33 (1986) 8822–8824.

[26] A.D. Becke, Density-functional exchange-energy approimation with correct asymptotic behavior, Phys. Rev. 38 (1988) 3098–3100.

[27] A. Schäfer, C. Huber, R. Ahlrichs, A. Schafer, C. Huber, R. Ahlrichs, Fully optimized contracted Gaussian basis sets of triple zeta valence quality for atoms Li to Kr Fully optimized contracted Gaussian basis sets of triple zeta valence quality for atoms Li to Kr, J. Chem. Phys. 100 (1994) 5829–5835, https://doi.org/10.1063/1.467146.

[28] A. Eckert, F. Klamt, COSMOthermX, 2016.

[29] G. Kresse, J. Hafner, Ab initio molecular dynamics for liquid metals, Phys. Rev. B 47 (1993) 558–561, https://doi.org/10.1103/PhysRevB.47.558.

[30] T. Brousse, B. Daniel, To Be or not to Be Pseudocapacitive ? J. Electrochem. Soc. 162 (2015) 5185–5189, https://doi.org/10.1149/2.0201505jes.

[31] P. Simon, Y. Gogotsi, B. Dunn, Where do batteries end and supercapacitors Begin ? Science 343 (80) (2014) 1210–1211, https://doi.org/10.1126/science.1249625.

[32] T.L. Greaves, C.J. Drummond, Protic ionic liquids: properties and applications, Chem, Rev 108 (2008) 206–237, https://doi.org/10.1021/cr068040u.

[33] J. Stoimenovski, E.I. Izgorodina, D.R. MacFarlane, Ionicity and proton transfer in protic ionic liquids, Phys. Chem. Chem. Phys. 12 (2010) 10341–10347, https://doi.org/10.1039/c0cp00239a.

[34] T.L. Amyes, S.T. Diver, J.P. Richard, F.M. Rivas, K. Toth, Formation and stability of N-heterocyclic carbenes in water: the carbon acid pKa of imidazolium cations in aqueous solution, J. Am. Chem. Soc. 126 (2004) 4366–4374, https://doi.org/10.1021/ja039890j.

[35] A.I. Frolov, K. Kirchner, T. Kirchner, M.V. Fedorov, Molecular-scale insights into the mechanisms of ionic liquids interactions with carbon nanotubes, Faraday Discuss 154 (2012) 235–247, https://doi.org/10.1039/c1fd00080b.

[36] A. Elbourne, S. McDonald, K. Voïchovsky, F. Endres, G.G. Warr, R. Atkin, Nanostructure of the ionic liquid-graphite stern layer, ACS Nano 9 (2015) 7608–7620, https://doi.org/10.1021/acsnano.5b02921.

[37] H.A. Mosqueda, O. Crosnier, L. Athouël, Y. Dandeville, Y. Scudeller, P. Guillemet, D.M. Schleich, T. Brousse, Electrolytes for hybrid carbon-MnO_2 electrochemical capacitors, Electrochim. Acta 55 (2010) 7479–7483, https://doi.org/10.1016/j.electacta.2010.01.022.

[38] A. Balducci, D. Belanger, T. Brousse, J.W. Long, W. Sugimoto, Perspective—a guideline for reporting performance metrics with electrochemical capacitors: from electrode materials to full devices, J. Electrochem. Soc. 164 (2017) A1487–A1488, https://doi.org/10.1149/2.0851707jes.

[39] S. Trasatti, Effect of the nature of the metal on the dielectric properties of polar liquids at the interface with electrodes. A phenomenological approach, J. Electroanal. Chem. 123 (1981) 121–139, https://doi.org/10.1016/S0022-0728(81)80047-2.

[40] M. Agostini, M. Sadd, S. Xiong, C. Cavallo, J. Heo, J.H. Ahn, A. Matic, Designing a safe electrolyte enabling long-life Li/S batteries, ChemSusChem 12 (2019) 4176–4184, https://doi.org/10.1002/cssc.201901770.